INTERNATIONAL JOURNAL FOR NUMERICAL METHODS IN FLUIDS, VOL. 15, 925–952 (1992)

NUMERICAL SOLUTION OF TRANSONIC FULL-POTENTIAL-EQUIVALENT EQUATIONS IN VON MISES CO-ORDINATES

C.-F. AN AND R. M. BARRON

Department of Mathematics and Statistics and Fluid Dynamics Research Institute, University of Windsor, Windsor, Ontario, Canada N9B 3P4

SUMMARY

In this paper a new approach to calculate transonic flows is developed. A set of full-potential-equivalent equations in the von Mises co-ordinate system is formulated under the irrotationality and isentropic assumptions. The emphasis is placed on supercritical flow, in which the treatment of embedded shock waves is crucial to get convergent solutions. Shock jump conditions are employed and shock point operators (SPOs) are constructed in the body-fitting streamline co-ordinate system. SPOs and a type-dependent difference scheme are applied to solve the 'main' equation for the 'main' variable, the streamline ordinate y. A number of 'secondary' equations are deduced for the corresponding 'secondary' variables. An optimal combination for the 'secondary' variable, its equation and related difference scheme is selected to be the generalized density R, its linear equation and the Crank–Nicolson scheme. Numerical results show that the present approach gives good agreement with experimental data and other computational work for NACA0012 and biconvex aerofoils in both subcritical and supercritical ranges.

KEY WORDS CFD Potential transonic flow Streamwise co-ordinates Shock point operator

1. INTRODUCTION

Transonic flows are very often encountered in compressible flows, such as the flows around aerofoils, wings, through nozzle throats, cascade blades or past blunt bodies, etc. Thus, in the past two decades, transonic flow computation has been an upsurging topic for CFD workers in the aeronautical and applied mathematical communities. The history of its development may be broken down into three stages.

TSD stage. In 1971 Murman and Cole[1] first developed a type-dependent finite difference relaxation method and successfully solved the mixed-type transonic small-disturbance (TSD) equation. Subsequently Murman and Krupp[2] and Murman[3] improved the scheme, analysed the shock jump conditions and proposed the concept of shock point operator. After that there were many advances on the TSD equation (see e.g. References 4 and 5).

FP stage. In 1974 Jameson[6] extended Murman's[3] scheme and constructed his rotated difference scheme to solve the full-potential (FP) equation in the transonic regime. Since then transonic full-potential calculations have been developed considerably.[7–10]

Euler stage. In the early 1970s Magnus and Yoshihara[11] solved the Euler equations in the transonic range. However, the computer time was too much for the method to be useful. After

0271–2091/92/200925–28$19.00

Received February 1991
Revised May 1992

1976 many other researchers[12–16] attempted to solve the steady Euler equations by seeking the time-asymptotic solution of the unsteady Euler equations. The approach is now referred to as a time-dependent technique. On the other hand, quite a few researchers attacked the Euler equations from another side, namely the streamfunction–vorticity formulation, and solved it as an alternative to the steady Euler equations.[17–20]

In general, Euler solvers are more accurate, but more complicated and consume more computer time than the full-potential solvers. Therefore, in spite of the recent active efforts on Euler solvers, the full-potential calculations are still more attractive and widely used in practical transonic computation owing to their simplicity, efficiency and accuracy. The purpose of this paper is to report some transonic calculations at the FP stage.

The von Mises transformation is a classical transformation in fluid mechanics. After the transformation the co-ordinates become body-fitting ones and it is easy to obtain streamlines, so this transformation is especially convenient for aerodynamic design problems. Moreover, some boundary conditions after the transformation are Dirichlet-type, which is believed to provide a faster convergence rate for an iterative solution process.

Barron[21] connected Martin's approach[22] with the von Mises transformation and successfully solved the resulting elliptic equation to simulate the incompressible potential flow past an aerofoil. Later on[23,24] Barron's method[21] was extended to compressible flow with some promising results, especially for subcritical transonic flows.

In this paper a new approach to calculate transonic flows is developed. Emphasis is placed on the supercritical case, in which the treatment of an embedded supersonic pocket, partly bounded by a shock wave, is crucial to get acceptable convergent solutions.

Starting from the 2D steady Euler equations, through the introduction of the streamfunction and the von Mises transformation, a set of Euler-equivalent equations in the von Mises co-ordinate system is deduced. With the assumptions of irrotationality and the isentropic condition, a number of sets of full-potential-equivalent equations are formulated.

In each set of equations the 'main' equation is a second-order, non-linear partial differential equation for a 'main' geometric variable, namely the streamline ordinate y, as a function of abscissa x and streamfunction ψ. This 'main' equation has Dirichlet boundary conditions (for the analysis problem) and is coupled with one of the following 'secondary' variables: density ρ, generalized density R, squared Mach number M^2, x-velocity component u or reciprocal of density σ. All these 'secondary' variables as functions of x and ψ are solved using a corresponding 'secondary' equation of the proper set.

To get a numerical solution of the 'main' equation which is mathematically and physically consistent and well-classified, Murman and Cole's type-dependent scheme[1] is applied. To handle the embedded shock wave properly, a shock jump condition and a shock point operator (SPO) in von Mises co-ordinates are deduced using Murman's[3] ideas as a guide.

The 'secondary' equations are either first-order partial differential equations or first-order ordinary differential equations for the corresponding 'secondary' variables. Various difference schemes have been tested, including explicit, implicit, Crank–Nicolson, type-dependent and type-dependent with SPO, to solve the 'secondary' equation. The optimal 'secondary' variable, equation and scheme are selected after some computer experimentation. Generalized density R, its linear equation and the Crank–Nicolson scheme are recommended as the optimal combination.

The computed results from the recommended combination are compared with experimental data and other computations. Some discussion, suggestion and concluding remarks are given at the end of this paper.

2. MATHEMATICAL FORMULATION

2.1. Euler-equivalent equations

The governing equations of 2D, steady, inviscid flows are the Euler equations

$$\begin{pmatrix} \rho u \\ \rho u^2 + p \\ \rho uv \\ \rho uH \end{pmatrix}_x + \begin{pmatrix} \rho v \\ \rho uv \\ \rho v^2 + p \\ \rho vH \end{pmatrix}_y = 0, \tag{1a}$$

$$H = \frac{\gamma}{\gamma - 1}\frac{p}{\rho} + \frac{u^2 + v^2}{2}, \tag{1b}$$

where ρ is the density, u and v are the velocity components in the x- and y-directions respectively, p is the pressure, H is the total enthalpy per unit mass and γ is the ratio of specific heats. The dependent variables are normalized by the freestream density ρ_∞, speed q_∞ and dynamic pressure head $\rho_\infty q_\infty^2$. The independent variables x and y are scaled by a characteristic length, e.g. the chord length of the aerofoil.

Introducing the streamfunction ψ such that

$$\psi_y = \rho u, \qquad \psi_x = -\rho v \tag{2}$$

and substituting (2) into (1), one gets

$$\begin{pmatrix} \psi_y^2/\rho + p \\ -\psi_x\psi_y/\rho \\ \psi_y H \end{pmatrix}_x + \begin{pmatrix} -\psi_x\psi_y/\rho \\ \psi_x^2/\rho + p \\ -\psi_x H \end{pmatrix}_y = 0, \tag{3a}$$

$$H = \frac{\gamma}{\gamma - 1}\frac{p}{\rho} + \frac{\psi_x^2 + \psi_y^2}{2\rho^2}. \tag{3b}$$

The first component equation in (1a), the continuity equation, is satisfied automatically by introduction of the streamfunction. Thus only three equations are left, with three unknowns ψ, ρ and p.

If we interchange the roles of dependent variable ψ and independent variable y and keep the role of independent variable x invariant, then we have in fact introduced the von Mises transformation:

$$\phi = x, \quad \psi = \psi(x, y) \qquad \text{or} \qquad x = \phi, \quad y = y(\phi, \psi). \tag{4}$$

The Jacobian of the transformation is

$$J = \left.\frac{\partial(x, y)}{\partial(\phi, \psi)}\right|_{\phi = x} = y_\psi \tag{5}$$

and the differential operators are

$$\frac{\partial}{\partial x} = \frac{\partial}{\partial \phi} + \psi_x \frac{\partial}{\partial \psi} \quad \text{and} \quad \frac{\partial}{\partial y} = \psi_y \frac{\partial}{\partial \psi} \quad \text{when } \phi = x. \tag{6}$$

Acting (6) on y gives

$$\psi_x = -\frac{y_\phi}{y_\psi}, \qquad \psi_y = \frac{1}{y_\psi}. \tag{7}$$

Thus the differential operators become

$$\frac{\partial}{\partial x} = \frac{\partial}{\partial \phi} - \frac{y_\phi}{y_\psi}\frac{\partial}{\partial \psi}, \qquad \frac{\partial}{\partial y} = \frac{1}{y_\psi}\frac{\partial}{\partial \psi}. \tag{8}$$

Using (7) and (8) in (3) and simplifying, one gets

$$\begin{pmatrix} 1/\rho y_\psi + p y_\psi \\ y_\phi/\rho y_\psi \\ H \end{pmatrix}_\phi + \begin{pmatrix} -p y_\phi \\ p \\ 0 \end{pmatrix}_\psi = 0, \tag{9a}$$

$$H = \frac{\gamma}{\gamma - 1}\frac{p}{\rho} + \frac{1 + y_\phi^2}{2\rho^2 y_\psi^2}, \tag{9b}$$

where $\phi = x$.

The third equation in (9a), $H_\phi = 0$, means that the total enthalpy H is invariant along a streamline. For a flow problem with uniform freestream the total enthalpy H is also invariant along a line other than a streamline in the freestream. Therefore $H =$ constant throughout the flow field. This is the *isoenergetic* or *homoenergetic* assumption made by most Euler solver researchers. The constant can be evaluated at the freestream condition as

$$H = H_\infty = \frac{1}{\gamma - 1}\frac{1}{M_\infty^2} + \frac{1}{2}. \tag{10}$$

Finally, for 2D, steady, inviscid flows the governing *Euler-equivalent equations* in the von Mises co-ordinate system are

$$\left(\frac{1}{\rho y_\psi} + y_\psi p\right)_x - (y_x p)_\psi = 0, \tag{11a}$$

$$\left(\frac{y_x}{\rho y_\psi}\right)_x + p_\psi = 0, \tag{11b}$$

$$\frac{\gamma}{\gamma - 1}\frac{p}{\rho} + \frac{1 + y_x^2}{2\rho^2 y_\psi^2} = H_\infty. \tag{11c}$$

Equations (11a) and (11b) are x-momentum and y-momentum equations respectively and the energy equation is replaced by an algebraic equation (11c) for p and ρ. These three equations contain three unknowns, i.e. density ρ, pressure p and streamline ordinate y, as functions of abscissa x and streamfunction ψ.

2.2. *Full-potential-equivalent equations*

The Euler-equivalent equations (11) are not easy to solve even though they are kept in conservative form and the energy equation has been simplified to an algebraic equation via the homoenergetic assumption. However, for many practical transonic problems the flow can be assumed irrotational and isentropic. In this case the irrotationality condition

$$\omega = v_x - u_y = 0 \tag{12}$$

and the isentropic relation

$$p=\rho^{\gamma}/\gamma M_{\infty}^{2} \tag{13}$$

can be introduced.

Using the von Mises transformation, (12) becomes

$$(y_{\psi}v)_x-(y_x v+u)_{\psi}=0.$$

From (2) and (7),

$$\frac{v}{u}=-\frac{\psi_x}{\psi_y}=y_x \quad \text{(note that } \phi=x\text{)},$$

so the irrotationality condition becomes

$$(y_x y_{\psi} u)_x-[(1+y_x^2)u]_{\psi}=0 \tag{14}$$

or

$$\left(\frac{y_x}{\rho}\right)_x-\left(\frac{1+y_x^2}{\rho y_{\psi}}\right)_{\psi}=0, \tag{15}$$

where $\rho u y_{\psi}=1$ has been employed.

Therefore a set of so-called full-potential-equivalent equations in the von Mises co-ordinate system is composed of the x-momentum equation (11a), the y-momentum equation (11b), the isentropic relation (13) and the irrotationality condition (15).

To simplify the formulation further, let us differentiate the isentropic relation (13) w.r.t. x and ψ:

$$p_x=\frac{\rho^{\gamma-1}}{M_{\infty}^2}\rho_x, \qquad p_{\psi}=\frac{\rho^{\gamma-1}}{M_{\infty}^2}\rho_{\psi}. \tag{16}$$

Substituting (16) into (11a), the x-momentum equation becomes

$$-y_{x\psi}+y_{\psi}\left(y_{\psi}^2\frac{\rho^{\gamma+1}}{M_{\infty}^2}-1\right)\frac{\rho_x}{\rho}-y_x y_{\psi}^2\frac{\rho^{\gamma+1}}{M_{\infty}^2}\frac{\rho_{\psi}}{\rho}=0. \tag{17}$$

Similarly, the y-momentum equation (11b) becomes

$$y_{\psi}y_{xx}-y_x y_{x\psi}-y_x y_{\psi}\frac{\rho_x}{\rho}+y_{\psi}^2\frac{\rho^{\gamma+1}}{M_{\infty}^2}\frac{\rho_{\psi}}{\rho}=0. \tag{18}$$

The irrotationality condition (15) itself gives

$$y_{\psi}^2 y_{xx}-2y_x y_{\psi}y_{x\psi}+(1+y_x^2)y_{\psi\psi}-y_x y_{\psi}^2\frac{\rho_x}{\rho}+y_{\psi}(1+y_x^2)\frac{\rho_{\psi}}{\rho}=0 \tag{19}$$

after expansion.

Proper combinations of these three equations (17)–(19) produce a number of sets of equations which can be used to solve for y and ρ. For example, solving for ρ_x/ρ and ρ_{ψ}/ρ from (17) and (18), plugging them into (19) and simplifying the resulting equation, one gets

$$(y_{\psi}^2-K)y_{xx}-2y_x y_{\psi}y_{x\psi}+(1+y_x^2)y_{\psi\psi}=0, \tag{20a}$$

where

$$K=M_{\infty}^2/\rho^{\gamma+1} \tag{20b}$$

is referred to as the 'compressibility parameter'. Eliminating the $y_{x\psi}$-term from (17) and (18), one

gets

$$y_x y_\psi^2 (\rho^{\gamma+1})_x - y_\psi (1+y_x^2)(\rho^{\gamma+1})_\psi = (\gamma+1) M_\infty^2 y_{xx} \tag{21}$$

and equation (17) itself can be rewritten as

$$y_\psi \left(y_\psi^2 - \frac{M_\infty^2}{\rho^{\gamma+1}} \right) (\rho^{\gamma+1})_x - y_x y_\psi^2 (\rho^{\gamma+1})_\psi = (\gamma+1) M_\infty^2 y_{x\psi}. \tag{22}$$

Substituting y_{xx} in (21) and $y_{x\psi}$ in (22) into (19) gives

$$y_x \left(y_\psi^2 - \frac{M_\infty^2}{\rho^{\gamma+1}} \right) (\rho^{\gamma+1})_x + y_\psi \left((1-y_x^2) - \frac{M_\infty^2}{\rho^{\gamma+1}} \frac{1+y_x^2}{y_\psi^2} \right) (\rho^{\gamma+1})_\psi = (\gamma+1) M_\infty^2 \frac{1+y_x^2}{y_\psi^2} y_{\psi\psi}. \tag{23}$$

The 'main' equation (20) is a second-order non-linear partial differential equation for the streamline ordinate y, and it is coupled with another unknown, the density ρ. The type of this 'main' equation is mixed depending on the local flow behaviour. In fact, the discriminant of equation (20) is

$$\Delta = 4 y_\psi^2 (M^2 - 1), \tag{24}$$

where the squared local Mach number is

$$M^2 = \frac{M_\infty^2}{\rho^{\gamma+1}} \frac{1+y_x^2}{y_\psi^2}. \tag{25}$$

Hence, if the local flow is supersonic, then $M^2 > 1$ and $\Delta > 0$, so that equation (20) must be hyperbolic. In contrast, if the local flow is subsonic, equation (20) is elliptic. In other words, the mathematical classification of equation (20) is consistent with the physical meaning of the flow. This significant property of the equation for y creates the possibility of applying the type-dependent difference scheme originally developed by Murman and Cole[1] for TSD problems.

It should be mentioned that equation (20) was first obtained and classified by Naeem and Barron.[24] Dulikravich[25] also got a similar equation to (20) with a different-scaled compressibility parameter. If $K \to 0$, then equation (20) reduces to the incompressible flow equation

$$y_\psi^2 y_{xx} - 2 y_x y_\psi y_{x\psi} + (1+y_x^2) y_{\psi\psi} = 0. \tag{26}$$

This equation was obtained by Barron.[21] Greywall[26] deduced the same equation by a different method.

In order to find a proper 'secondary' equation to solve for the 'secondary' variable ρ, any of the above three equations (21)–(23) can be chosen to construct a complete set of equations. However, to simplify the formulation, define the generalized density

$$R = \rho^{\gamma+1}. \tag{27}$$

Then equations (20)–(23) and (25) become

$$(y_\psi^2 - K) y_{xx} - 2 y_x y_\psi y_{x\psi} + (1+y_x^2) y_{\psi\psi} = 0, \tag{28a}$$

where

$$K = M_\infty^2 / R, \tag{28b}$$

$$y_x y_\psi^2 R_x - y_\psi (1+y_x^2) R_\psi = (\gamma+1) M_\infty^2 y_{xx}, \tag{29}$$

$$y_\psi \left(y_\psi^2 - \frac{M_\infty^2}{R} \right) R_x - y_x y_\psi^2 R_\psi = (\gamma+1) M_\infty^2 y_{x\psi}, \tag{30}$$

$$y_x\left(y_\psi^2-\frac{M_\infty^2}{R}\right)R_x+y_\psi^2\left(1-y_x^2-\frac{M_\infty^2}{R}\frac{1+y_x^2}{y_\psi^2}\right)R_\psi=(\gamma+1)M_\infty^2\frac{1+y_x^2}{y_\psi^2}y_{\psi\psi}, \tag{31}$$

$$M^2=\frac{M_\infty^2}{R}\frac{1+y_x^2}{y_\psi^2}. \tag{32}$$

Equation (29) can also be rewritten in the 'conservative' form

$$(y_xR)_x-\left(\frac{1+y_x^2}{y_\psi}R\right)_\psi=(\gamma+2)M_\infty^2\frac{y_{xx}}{y_\psi^2}. \tag{33}$$

All the above 'secondary' equations (29)–(31) and (33) are first-order partial differential equations and can be solved for the 'secondary' variable R. However, only equation (29) seems to be the simplest one because it is linear. Thus why do we not choose it first to solve for R? Equation (29) can be solved (marched) from an initial data line other than its characteristic curve as long as y and its derivatives are known. In fact, the slope of the characteristics of equation (29) is

$$\frac{\mathrm{d}\psi}{\mathrm{d}x}=-\frac{1+y_x^2}{y_xy_\psi}. \tag{34}$$

At infinity, $y_x\to0$ and $y_\psi\to1$, so $\mathrm{d}\psi/\mathrm{d}x\to\infty$. Thus both the left and right boundaries at infinity are characteristic curves and therefore cannot serve as initial data lines. Fortunately, the horizontal boundary at infinity meets the requirement of such an initial line. Hence we can march (29) to the aerofoil from the top boundary for the upper half-plane and from the bottom boundary for the lower half-plane.

The boundary conditions for the 'main' equation (28) are very simple Dirichlet ones. For a symmetric aerofoil at zero incidence,

$$y=f(x) \quad \text{on the aerofoil,} \tag{35a}$$

$$y=\psi \quad \text{at infinity,} \tag{35b}$$

$$y=0 \quad \text{on the symmetry line,} \tag{35c}$$

where $f(x)$ is the shape function of the aerofoil. For the 'secondary' equation (29), both initial and boundary conditions are

$$R=1 \quad \text{at infinity.} \tag{36}$$

2.3. Alternative 'secondary' equations

Apart from equations (29)–(31) and (33), a number of other 'secondary' equations can be found to solve for the corresponding 'secondary' variables. For example, if we eliminate the R_ψ-term from (29) and (30), we can get a first-order ordinary differential equation for R:

$$R_x=\frac{\gamma+1}{2}M_\infty^2\left(\frac{M_\infty^2}{R}\frac{1+y_x^2}{y_\psi^2}-1\right)^{-1}\left(\frac{1+y_x^2}{y_\psi^2}\right)_x. \tag{37}$$

Similarly, eliminating the R_x-term from (30) and (31), we have

$$R_\psi=\frac{\gamma+1}{2}M_\infty^2\left(\frac{M_\infty^2}{R}\frac{1+y_x^2}{y_\psi^2}-1\right)^{-1}\left(\frac{1+y_x^2}{y_\psi^2}\right)_\psi. \tag{38}$$

It is interesting that (37) and (38) are astonishingly similar and symmetric.

At a shock wave it is better to replace (37) by the Rankine–Hugoniot relation

$$R^+ = \left[\frac{1}{R}\left(\frac{(\gamma+1)\,(1+y_x^2)}{2(\gamma-1)H_\infty y_\psi^2}\right)^{\gamma+1}\right]^- \tag{39}$$

where the superscripts '+' and '−' represent the downstream and upstream sides of the shock wave respectively.

Equation (37) accompanied by (39) and equation (38) can be marched along the x- and ψ-directions step-by-step.

Furthermore, if we differentiate (29) w.r.t. ψ and (30) w.r.t. x and subtract them to eliminate third-order y-derivatives $y_{x\psi x}$ and $y_{x\psi x}$, we can get a second-order, but non-homogeneous, partial differential equation for R with the same differential operator as in the y-equation (28):

$$\left(y_\psi^2 - \frac{M_\infty^2}{R}\right)R_{xx} - 2y_x y_\psi R_{x\psi} + (1+y_x^2)R_{\psi\psi} = G, \tag{40a}$$

where

$$G = \frac{\gamma+1}{2}M_\infty^2 \frac{\left\{(y_x y_\psi^2)_\psi - \left[y_\psi\left(y_\psi^2 - \frac{M_\infty^2}{R}\right)\right]_x\right\}\left(\frac{1+y_x^2}{y_\psi^2}\right)_x + \{(y_x y_\psi^2)_x - [y_\psi(1+y_x^2)]_\psi\}\left(\frac{1+y_x^2}{y_\psi^2}\right)_\psi}{y_\psi\left(\frac{M_\infty^2}{R}\frac{1+y_x^2}{y_\psi^2} - 1\right)}. \tag{40b}$$

The boundary condition for R on the aerofoil is

$$R = \left[1 + \frac{\gamma-1}{2}M^2\left(1 - \frac{1+f'^2(x)}{R^{2/(\gamma+1)}y_\psi^2}\right)\right]^{(\gamma+1)/(\gamma-1)}. \tag{41}$$

We can see that both differential equation (40) and boundary condition (41) are non-linear.

All the above R-equations (37), (38) and (40) can be used as 'secondary' equations to solve for R to update the compressibility parameter $K = M_\infty^2/R$ in the 'main' equation (28).

On the other hand, using the R–M^2 relation (32) in equation (37), we get a first-order ordinary differential equation for M^2:

$$(M^2)_x = \frac{M^2\{1+[(\gamma-1)/2]M^2\}}{1-M^2}\left[\ln\left(\frac{1+y_x^2}{y_\psi^2}\right)\right]_x. \tag{42}$$

However, at a shock wave equation (42) should be replaced by the Rankine–Hugoniot relation

$$(M^2)^+ = \frac{1+[(\gamma-1)/2]\,(M^2)^-}{\gamma(M^2)^- - (\gamma-1)/2}. \tag{43}$$

Accordingly, the compressibility parameter in equations (28) should be expressed as

$$K = M^2\frac{y_\psi^2}{1+y_x^2}. \tag{44}$$

Superficially, this set of equations seems to be a good formulation, but it is too early to conclude its success before performing some computations.

Next we will just list some of the other alternative sets of full-potential-equivalent equations for reference without giving any derivations. In each set the 'main' equation for y takes the form of

(28) and the compressibility K takes different forms in different sets:

$$y\text{–}\rho \text{ set} \begin{cases} K = M_\infty^2/\rho^{\gamma+1}, & (45a) \\ y_\psi^2\left(y_\psi^2\dfrac{\rho^{\gamma+1}}{M_\infty^2}-1+(\gamma-1)y_x^2\right)\rho_x - y_x y_\psi\left(y_\psi^2\dfrac{\rho^{\gamma+1}}{M_\infty^2}+(\gamma-1)(1+y_x^2)\right)\rho_\psi & \\ -\dfrac{\gamma-1}{2}\left[y_\psi^2(y_x^2)_x+\left(\dfrac{1}{\gamma-1}-2y_x^2\right)(y_\psi^2)_x+\dfrac{y_x}{y_\psi}(1+y_x^2)(y_\psi^2)_\psi\right]\rho=0; & (45b) \end{cases}$$

$$y\text{–}\sigma \text{ set} \begin{cases} K = M_\infty^2\sigma^{\gamma+1}, & (46a) \\ (y_x\sigma)_x-\left(\dfrac{1+y_x^2}{y_\psi}\sigma\right)_\psi=0, & (46b) \\ \sigma=1/\rho; & (46c) \end{cases}$$

$$y\text{–}u \text{ set} \begin{cases} K = M_\infty^2 y_\psi^{\gamma+1}u^{\gamma+1}, & (47a) \\ (y_x y_\psi u)_x-[u(1+y_x^2)]_\psi=0; & (47b) \end{cases}$$

$$y\text{–}u\text{–}\rho \text{ set} \begin{cases} K = M_\infty^2/\rho^{\gamma+1}, & (48a) \\ (y_x y_\psi u)_x-[(1+y_x^2)u]_\psi=0, & (48b) \\ \rho=\left(1+\dfrac{\gamma-1}{2}M_\infty^2\,[1-(1+y_x^2)u^2]\right)^{1/(\gamma-1)}. & (48c) \end{cases}$$

It can be pointed out that although these formulations are theoretically rational, the computer calculations may fail to give acceptable results. However, it is difficult to undergo the tedious and time-consuming work of running all possible combinations of these sets of equations with various schemes and relaxation parameters on a computer. Thus we have to select an optimal combination of a 'best' secondary variable, a 'best' secondary equation and a 'best' difference scheme. Regardless, it is natural and logical to choose the simplest set of equations (28) and (29) to first attack the problem.

3. NUMERICAL ALGORITHM

3.1. Type-dependent scheme

Because equation (28) is conveniently classified to hyperbolic or elliptic type depending on the local supersonic or subsonic flow properties, it is permissible to apply Murman and Cole's type-dependent scheme to solve (28) for y as long as R is known.

Equation (28) can be rewritten as

$$A_1 y_{xx} + A_2 y_{x\psi} + A_3 y_{\psi\psi} = 0, \tag{49a}$$

where

$$A_1 = y_\psi^2 - K, \qquad K = M_\infty^2 / R, \tag{49b}$$

$$A_2 = -2 y_x y_\psi, \tag{49c}$$

$$A_3 = 1 + y_x^2. \tag{49d}$$

The type-dependent scheme reads

$$\{A_1 [v\Delta_x + (1-v)\nabla_x]\nabla_x + A_2 [v\delta_x + (1-v)\nabla_x]\delta_\psi + A_3 \delta_{\psi\psi}\} y_{i,j} = 0, \tag{50a}$$

where Δ, ∇ and δ are forward, backward and central difference operators and

$$v = \begin{cases} 1 & \text{if local flow is subsonic,} \\ 0 & \text{if local flow is supersonic,} \end{cases} \tag{50b}$$

is a switch parameter.

Expanding (50a) and rearranging the terms, one gets

$$A y_{i,j-1} + B y_{i,j} + C y_{i,j+1} = \text{RHS}, \quad i = 2, 3, \ldots, I_{\max-1}, \quad j = 2, 3, \ldots, J_{\max-1} \tag{51a}$$

where

$$A = \beta^2 A_3 - \frac{1-v}{2} \beta A_2, \qquad \beta = \frac{\Delta x}{\Delta \psi}, \tag{51b}$$

$$B = -2\beta^2 A_3 + (1-3v) A_1, \tag{51c}$$

$$C = \beta^2 A_3 + \frac{1-v}{2} \beta A_2, \tag{51d}$$

$$\begin{aligned} \text{RHS} = & -v A_1 (y_{i+1,j} + y_{i-1,j}) + (1-v) A_1 (2y_{i-1,j} - y_{i-2,j}) \\ & - \frac{v}{4} \beta A_2 (y_{i+1,j+1} - y_{i+1,j-1} - y_{i-1,j+1} + y_{i-1,j-1}) \\ & + \frac{1-v}{2} \beta A_2 (y_{i-1,j+1} - y_{i-1,j-1}). \end{aligned} \tag{51e}$$

From (35) the boundary conditions are

$$y_{i,1} = \begin{cases} f(x_i) & \text{if } i_{\text{LE}} \leqslant i \leqslant i_{\text{TE}}, \\ 0 & \text{if } i < i_{\text{LE}} \text{ or } i > i_{\text{TE}}, \end{cases} \tag{52a}$$

$$y_{i,j} = \psi_j \quad \text{if } i = 1 \text{ or } I_{\max} \text{ or } j = J_{\max}. \tag{52b}$$

The system of difference equations (51) with boundary conditions (52) has a tridiagonal coefficient matrix, so the successive line overrelaxation (SLOR) procedure can be used. Along a vertical i fixed line, system (51) is relaxed and then a sweep from left to right is made. A simple tridiagonal solver is available to use, but an iterative procedure has to be applied owing to the non-linearity of the equations. The stencils of the type-dependent schemes and boundary conditions are shown in Figure 1.

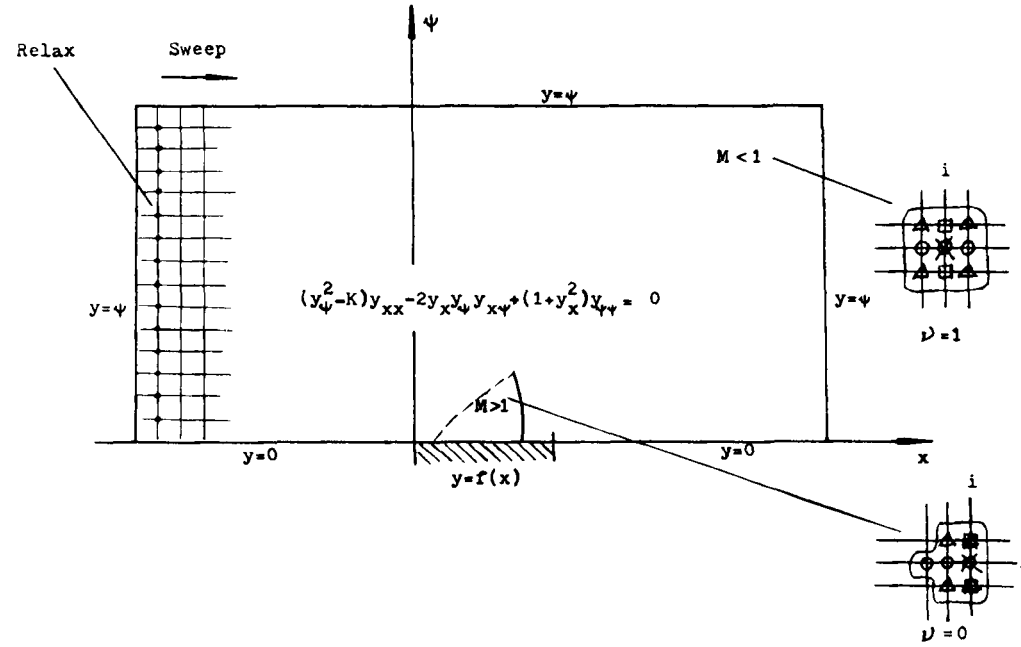

Figure 1. Type-dependent scheme and boundary conditions for y-equation

3.2. *Crank–Nicolson scheme*

As mentioned earlier, after $y(x, \psi)$ has been solved from the 'main' equation and y_x, y_ψ and y_{xx} have been properly differenced from y, the 'secondary' equation (29) can be solved for $R(x, \psi)$ by marching from the horizontal far-field boundary to the aerofoil.

Equation (29) can be rewritten as

$$B_1 R_x + B_2 R_\psi = B_3, \tag{53a}$$

where

$$B_1 = y_x y_\psi^2, \tag{53b}$$

$$B_2 = -y_\psi(1+y_x^2), \tag{53c}$$

$$B_3 = (\gamma+1)M_\infty^2 y_{xx}. \tag{53d}$$

The Crank–Nicolson difference scheme is an implicit, second-order-accurate and unconditionally stable difference scheme. Applying it to equation (53a) at point $(i, j+\frac{1}{2})$ gives

$$B_1 \frac{R_{i+1,j+1/2} - R_{i-1,j+1/2}}{2\Delta x} + B_2 \frac{R_{i,j+1} - R_{i,j}}{\Delta\psi} = B_3.$$

Evaluating each variable at level $j+\frac{1}{2}$ by the average on levels j and $j+1$, one gets

$$\tilde{A} R_{i-1,j} + \tilde{B} R_{i,j} + \tilde{C} R_{i+1,j} = \widetilde{\mathrm{RHS}}, \quad j = J_{\max-1}, \ldots, 3, 2, 1, \quad i = 2, 3, \ldots, I_{\max-1} \tag{54a}$$

where

$$\tilde{A} = -B_1, \tag{54b}$$

$$\tilde{B} = -4\beta B_2, \qquad \beta = \frac{\Delta x}{\Delta \psi}, \tag{54c}$$

$$\tilde{C} = B_1, \tag{54d}$$

$$\widetilde{\mathrm{RHS}} = \tilde{C}\, R_{i-1,j+1} + \tilde{B}\, R_{i,j+1} + \tilde{A}\, R_{i+1,j+1} + 4\Delta x B_3, \tag{54e}$$

with

$$B_1 = \tfrac{1}{2}[(y_x y_\psi^2)_{i,j} + (y_x y_\psi^2)_{i,j+1}], \tag{54f}$$

$$B_2 = -\tfrac{1}{2}\{[y_\psi(1+y_x^2)]_{i,j} + [y_\psi(1+y_x^2)]_{i,j+1}\}, \tag{54g}$$

$$B_3 = \frac{\gamma+1}{2} M_\infty^2 [(y_{xx})_{i,j} + (y_{xx})_{i,j+1}]. \tag{54h}$$

The system of difference equations (54) can be solved line-by-line horizontally from the far-field boundary to the aerofoil using SLOR with a tridiagonal solver, but no iterative procedure is needed at this stage owing to its linearity. The difference scheme stencil and boundary conditions are shown in Figure 2. The following points should be emphasized.

(i) The coefficient matrix of the system (54) is diagonally dominant at most grid lines. This fact guarantees the numerical solution of the system. In fact, for most grid points off the aerofoil surface, $y_x \approx 0$, $y_\psi \approx 1$ and β can be chosen equal to or greater than unity, then

$$|\tilde{B}| - (|\tilde{A}| + |\tilde{C}|) = 4\beta|B_2| - 2|B_1| \geqslant 2|y_\psi|[2(1+y_x^2) - |y_x y_\psi|] \geqslant 0. \tag{55}$$

This inequality is easily satisfied for most points. Only for points close to the aerofoil or shock wave may the inequality be violated. We should pay particular attention to those situations.

(ii) The marching process can only be carried out from the horizontal far-field boundary instead of the vertical far-field boundary or aerofoil surface, because R is easy to specify at infinity and, more importantly, the horizontal boundary is not a characteristic curve, while the left and right far-field boundaries are such curves.

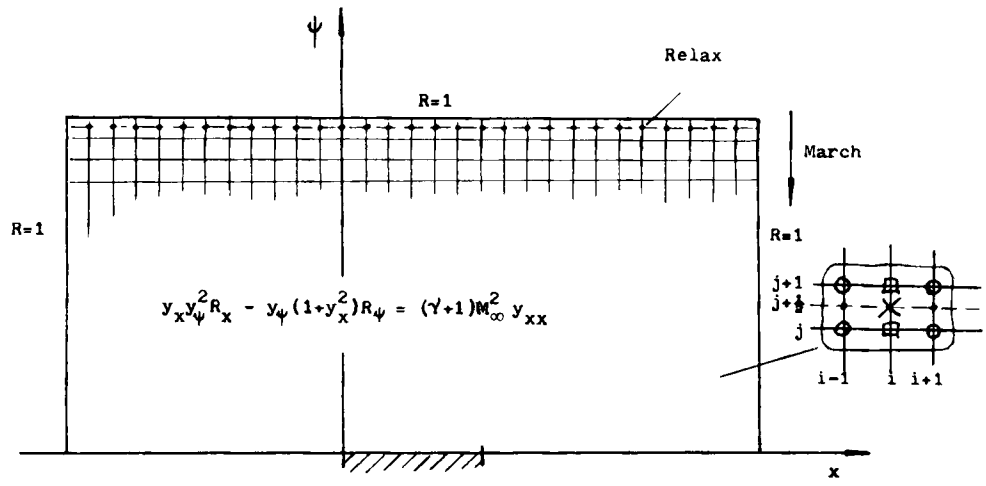

Figure 2. Crank–Nicolson scheme and boundary conditions for R-equation

(iii) The right-hand-side term in equation (53a) includes y_{xx}, which must be type-dependent differenced with SPOs (explained in the next subsection) to keep consistent with the case in the y-equation. However, for R_x and y_x, whether type-dependent differencing with SPOs is needed or not can be determined only after the numerical tests. A number of alternative schemes have been tested, including explicit, implicit, first-order and second-order type-dependent with and without SPOs, etc. It was found that the Crank–Nicolson scheme is the optimal one.

After R has been solved, the squared Mach number is calculated from (32) and the pressure coefficient is calculated from

$$C_p = \frac{2}{\gamma M_\infty^2}(R^{\gamma/(\gamma+1)} - 1). \tag{56}$$

3.3. *Shock wave treatment*

After some numerical tests it was found that the type-dependent scheme is effective to achieve good solutions for the subcritical case of transonic flows and for the supercritical case with very weak shock waves. However, for a supercritical transonic flow with moderate or strong shock wave the iterative procedure either fails to converge or is forced to be stopped owing to inaccurate intermediate values of the unknowns y and R.

In the early work of Murman and Cole[1] the shock jump conditions are automatically contained in their TSD formulation in the integral form. The sonic line and shock waves evolve naturally during the course of iteration. The shock is captured as part of the continuous solution and is smeared out over several grid points. Thus no special shock wave treatment is needed for their computation. Murman, in his later paper,[3] proposed the concept of shock point operator (SPO) for the TSD equations, but his SPO cannot be applied directly here. However, his analysis of the shock structure provides a useful hint for modification of the FP-equivalent equations. Next let us analyse our shock jump conditions, propose an SPO and apply it to solve the problem of supercritical FP transonic flow.

Shock jump conditions. Suppose an oblique shock with velocity V makes an angle β with the x-axis, u and v are Cartesian components of V, V_n and V_t are normal and tangential components of V and α is the angle of V with the x-axis. Superscripts '$-$' and '$+$' represent upstream and downstream of the shock. Then (Figure 3) the tangential shock wave relation $V_t^- = V_t^+$ gives

$$(v^+ - v^-)\sin\beta + (u^+ - u^-)\cos\beta = 0$$

or

$$\frac{v^+ - v^-}{u^+ - u^-} = -\cot\beta = -\left(\frac{dx}{dy}\right)_s. \tag{57}$$

The normal shock wave relation $\rho^- V_n^- = \rho^+ V_n^+$ gives

$$(\rho^+ u^+ - \rho^- u^-)\sin\beta - (\rho^+ v^+ - \rho^- v^-)\cos\beta = 0$$

or

$$\frac{\rho^+ u^+ - \rho^- u^-}{\rho^+ v^+ - \rho^- v^-} = \cot\beta = \left(\frac{dx}{dy}\right)_s, \tag{58}$$

where $(dx/dy)_s = \cot\beta$ is the slope of the shock wave. Equations (57) and (58) can be expressed in

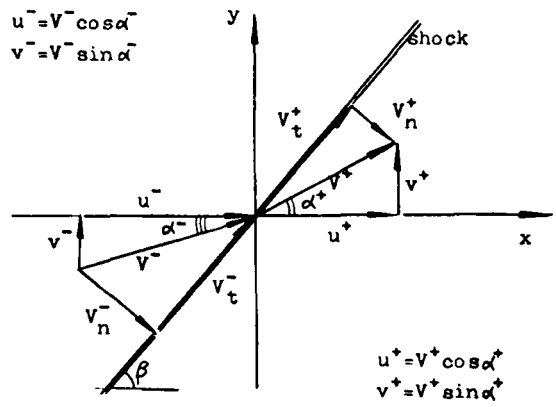

Figure 3. Shock jump conditions

the compact form

$$[v]+\left(\frac{\mathrm{d}x}{\mathrm{d}y}\right)_s[u]=0, \qquad [\rho u]-\left(\frac{\mathrm{d}x}{\mathrm{d}y}\right)_s[\rho v]=0,$$

where $[\cdot]$ represents the jump across the shock. Considering $\rho u y_\psi = 1$ and $v = y_x u$, we get the oblique shock jump conditions

$$\left[\frac{y_x}{\rho y_\psi}\right]+\left(\frac{\mathrm{d}x}{\mathrm{d}y}\right)_s\left[\frac{1}{\rho y_\psi}\right]=0, \tag{59a}$$

$$\left[\frac{1}{y_\psi}\right]-\left(\frac{\mathrm{d}x}{\mathrm{d}y}\right)_s\left[\frac{y_x}{y_\psi}\right]=0. \tag{59b}$$

For a normal shock, i.e. a shock whose plane is perpendicular to the x-axis, $(\mathrm{d}x/\mathrm{d}y)_s = 0$. The shock jump conditions are then reduced to

$$\left[\frac{y_x}{\rho y_\psi}\right]=0, \qquad \left[\frac{1}{y_\psi}\right]=0.$$

Finally, we get the normal shock jump conditions of the simplest form

$$\left[\frac{y_x}{\rho}\right]=0, \qquad [y_\psi]=0. \tag{60}$$

Shock point operator (SPO). The shock wave appearing in many transonic flow regions is approximately normal and we assume that it is an infinitely thin discontinuous surface located at point $(i-\frac{1}{2}, j)$ and perpendicular to the x-axis. From the previous paragraph, only y_x/ρ and y_ψ are continuous across this discontinuity, but y_x, y_{xx}, $y_{x\psi}$, ρ, R, M^2, etc. are not (see Figure 4). The normal shock jump conditions (60) are

$$y_\psi^+ = y_\psi^-, \qquad y_x^+ = y_x^- \frac{\rho^+}{\rho^-}. \tag{61}$$

The Rankine–Hugoniot relation for a normal shock is

$$\frac{\rho^+}{\rho^-} = \frac{[(\gamma+1)/2]\,(M^2)^-}{1+[(\gamma-1)/2]\,(M^2)^-}. \tag{62}$$

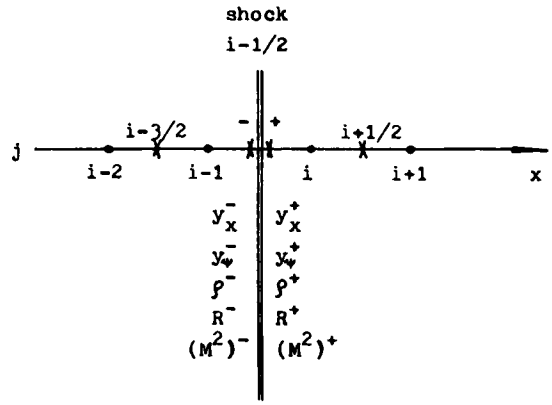

Figure 4. Shock point operator

The squared Mach number at $(i-\frac{1}{2}, j)^-$ can be evaluated by extrapolation from the two upstream points as

$$M^2_{i-1/2,j} = \tfrac{3}{2} M^2_{i-1,j} - \tfrac{1}{2} M^2_{i-2,j}. \tag{63}$$

Thus the shock jump conditions (61) can be rewritten as

$$y_\psi^+ = y_\psi^-, \qquad y_x^+ = \alpha_j y_x^-, \tag{64a}$$

where

$$\alpha_j = \left(\frac{\rho^+}{\rho^-}\right)_j = \frac{[(\gamma+1)/4]\,(3M^2_{i-1,j} - M^2_{i-2,j})}{1+[(\gamma-1)/4]\,(3M^2_{i-1,j} - M^2_{i-2,j})} \tag{64b}$$

is the density jump factor on the jth streamline. Furthermore, we can construct a difference scheme for y_x at a shock point $i = i_s$, i.e. the grid point just behind the shock:

$$\begin{aligned}(y_x)_{i,j} &= \tfrac{1}{2}[(y_x)_{i+1/2,j} + (y_x)^+_{i-1/2,j}] \\ &= \tfrac{1}{2}[(y_x)_{i+1/2,j} + \alpha_j (y_x)^-_{i-1/2,j}] \\ &= \frac{1}{2\Delta x}(y_{i+1,j} - y_{i,j} + \alpha_j y_{i-1,j} - \alpha_j y_{i-2,j}),\end{aligned} \tag{65}$$

where second-order difference formulae

$$(y_x)_{i+1/2,j} = \frac{1}{\Delta x}(y_{i+1,j} - y_{i,j}) \quad \text{and} \quad (y_x)^-_{i-1/2,j} = \frac{1}{\Delta x}(y_{i-1,j} - y_{i-2,j})$$

have been used. Similarly, for $i = i_s$,

$$(y_{xx})_{i,j} = \frac{1}{\Delta x^2}(y_{i+1,j} - y_{i,j} - \alpha_j y_{i-1,j} + \alpha_j y_{i-2,j}), \tag{66}$$

$$\begin{aligned}(y_{x\psi})_{i,j} = \frac{1}{4\Delta x \Delta \psi}(&y_{i+1,j+1} - y_{i+1,j-1} + y_{i,j+1} - y_{i,j-1} - 3y_{i-1,j+1} + 3y_{i-1,j-1} \\ &+ y_{i-2,j+1} - y_{i-2,j-1}).\end{aligned} \tag{67}$$

Equations (65)–(67) define so-called shock point operators in von Mises co-ordinates. Owing to the special treatment of the grid point at a shock wave, we have to revise the type-dependent scheme (51) for the y-equation and (54) for the R-equation.

Type-dependent scheme with SPOs. Based on the SPOs derived above, the system of difference equations corresponding to the 'main' equation (49a) for y is still of the same form as (51a), i.e.

$$Ay_{i,j-1}+By_{i,j}+Cy_{i,j+1}=\text{RHS}, \tag{68a}$$

but the coefficients and right-hand-side term are revised as

$$A=\beta^2 A_3-\begin{Bmatrix}(1-v)/2\\ \frac{1}{4}\end{Bmatrix}\beta A_2 \quad \begin{cases}\text{if } i\neq i_s,\\ \text{if } i=i_s,\end{cases} \tag{68b}$$

$$B=-2\beta^2 A_3+\begin{Bmatrix}1-3v\\ -1\end{Bmatrix}A_1 \quad \begin{cases}\text{if } i\neq i_s,\\ \text{if } i=i_s,\end{cases} \tag{68c}$$

$$C=\beta^2 A_3+\begin{Bmatrix}(1-v)/2\\ \frac{1}{4}\end{Bmatrix}\beta A_2 \quad \begin{cases}\text{if } i\neq i_s,\\ \text{if } i=i_s,\end{cases} \tag{68d}$$

$$\text{RHS}=\begin{cases}
-vA_1(y_{i+1,j}+y_{i-1,j})+(1-v)A_1(2y_{i-1,j}-y_{i-2,j})\\
\quad -\dfrac{v}{4}\beta A_2(y_{i+1,j+1}-y_{i+1,j-1}-y_{i-1,j+1}+y_{i-1,j-1})\\
\quad +\dfrac{1-v}{2}\beta A_2(y_{i-1,j+1}-y_{i-1,j-1}) \quad \text{if } i\neq i_s,\\
-A_1(y_{i+1,j}-\alpha_j y_{i-1,j}+\alpha_j y_{i-2,j})\\
\quad -\frac{1}{4}\beta A_2(y_{i+1,j+1}-y_{i+1,j-1}-3y_{i-1,j+1}\\
\quad +3y_{i-1,j-1}+y_{i-2,j+1}-y_{i-2,j-1}) \quad \text{if } i=i_s.
\end{cases} \tag{68e}$$

For the 'secondary' equation (53a) the corresponding difference equation, its coefficients and its RHS term take the same form as in equations (54a)–(54h), but the second derivative y_{xx} in equation (54h) should be approximated by a type-dependent difference scheme with shock point operator

$$(y_{xx})_{ij}=\begin{cases}\dfrac{v}{\Delta x^2}(y_{i+1,j}-2y_{i,j}+y_{i-1,j})+\dfrac{1-v}{\Delta x^2}(y_{i,j}-2y_{i-1,j}+y_{i-2,j}) & \text{if } i\neq i_s,\\ \dfrac{1}{\Delta x^2}(y_{i+1,j}-y_{i,j}-\alpha_j y_{i-1,j}+\alpha_j y_{i-2,j}) & \text{if } i=i_s,\end{cases} \tag{69}$$

where the switch parameter v is defined in equation (50b) and the density jump factor α_j is given by equation (64b).

Criterion of classifying points. In order to determine the local flow type at grid point (i,j), we have to check the flow property at two adjacent points, namely the current point (i,j) and the upstream point $(i-1,j)$. The criteria are shown in Table I. In computational practice the sonic point does not need to be distinguished because there is no jump across it, but the shock point must be identified carefully, and this is a key step to get a convergent solution.

Table I

$M^2_{i-1,j}$	$M^2_{i,j}$	Local flow type at (i,j)
<1	<1	Subsonic point
<1	>1	Sonic point
>1	>1	Supersonic point
>1	<1	Shock point

4. CLUSTERING TRANSFORMATION

In order to improve the accuracy by increasing the number of grid points on the surface of the aerofoil without consuming too much computer time, some kind of clustering (stretching) transformation can be applied to pack mesh points for larger-gradient regions and spread out mesh points for smaller-gradient regions.

Jones' algebraic stretching transformation[5] is a simple and effective one:

$$x = a\, e^{-b\xi^2} \tan \xi, \tag{70a}$$

$$\psi = d \tan \eta. \tag{70b}$$

A new variable Y can be introduced by

$$y = Y + \psi. \tag{71}$$

Substituting (70) and (71) into (28), we get

$$A_1 Y_{\xi\xi} + A_2 Y_{\xi\eta} + A_3 Y_{\eta\eta} + A_4 Y_\xi + A_5 Y_\eta = 0, \tag{72a}$$

where

$$A_1 = (Y_\eta + \psi_\eta)^2 - \tilde{K}, \qquad \tilde{K} = K\psi_\eta^2 = \frac{M_\infty^2}{R}\psi_\eta^2, \tag{72b}$$

$$A_2 = -2Y_\xi(Y_\eta + \psi_\eta), \tag{72c}$$

$$A_3 = Y_\xi^2 + x_\xi^2, \tag{72d}$$

$$A_4 = -\frac{x_{\xi\xi}}{x_\xi} A_1, \tag{72e}$$

$$A_5 = -\frac{\psi_{\eta\eta}}{\psi_\eta} A_3 \tag{72f}$$

and the squared Mach number is

$$M^2 = \frac{M_\infty^2}{R}\frac{\psi_\eta^2}{x_\xi^2}\frac{Y_\xi^2 + x_\xi^2}{(Y_\eta + \psi_\eta)^2}. \tag{73}$$

The normal shock jump conditions (60) become

$$\left[\frac{Y_\xi}{\rho x_\xi}\right] = 0, \qquad \left[\frac{Y_\eta}{\psi_\eta} + 1\right] = 0.$$

Because x_ξ and ψ_η are continuous everywhere, the shock jump conditions have the same form as (60), i.e.

$$\left[\frac{Y_\xi}{\rho}\right] = 0, \qquad [Y_\eta] = 0. \tag{74}$$

Similarly, we get SPOs for clustered co-ordinates:

$$Y_\eta^+ = Y_\eta^-, \qquad Y_\xi^+ = \alpha_j Y_\xi^-, \tag{75a}$$

where

$$\alpha_j = \left(\frac{\rho^+}{\rho^-}\right)_j = \frac{[(\gamma+1)/4]\,(3M_{i-1,j}^2 - M_{i-2,j}^2)}{1+[(\gamma-1)/4]\,(3M_{i-1,j}^2 - M_{i-2,j}^2)} \tag{75b}$$

is the density jump factor on the jth streamline and

$$(Y_\xi)_{i,j} = \frac{1}{2\Delta\xi}(Y_{i+1,j} - Y_{i,j} + \alpha_j Y_{i-1,j} - \alpha_j Y_{i-2,j}), \tag{76a}$$

$$(Y_{\xi\xi})_{i,j} = \frac{1}{\Delta\xi^2}(Y_{i+1,j} - Y_{i,j} - \alpha_j Y_{i-1,j} + \alpha_j Y_{i-2,j}), \tag{76b}$$

$$(Y_{\xi\eta})_{i,j} = \frac{1}{4\Delta\xi\Delta\eta}(Y_{i+1,j+1} - Y_{i+1,j-1} + Y_{i,j+1} - Y_{i,j-1} - 3Y_{i-1,j+1} + 3Y_{i-1,j-1} + Y_{i-2,j+1} - Y_{i-2,j-1}). \tag{76c}$$

Using the type-dependent scheme with SPOs on equation (72a), we get the following system of difference equations with tridiagonal coefficient matrix:

$$AY_{i,j-1} + BY_{i,j} + CY_{i,j+1} = \text{RHS}, \quad i = 2, 3, \ldots, I_{\max-1}, \quad J = 2, 3, \ldots, J_{\max-1}, \tag{77a}$$

where

$$A = \beta^2 A_3 - \tfrac{1}{2}\beta\Delta\xi A_5 - \begin{Bmatrix}(1-v)/2\\ \tfrac{1}{4}\end{Bmatrix}\beta A_2 \quad \begin{cases}\text{if } i \neq i_s,\\ \text{if } i = i_s,\end{cases} \tag{77b}$$

$$B = -2\beta^2 A_3 + \begin{Bmatrix}1-3v\\ -1\end{Bmatrix} A_1 + \begin{Bmatrix}1-v\\ -\tfrac{1}{2}\end{Bmatrix}\Delta\xi A_4 \quad \begin{cases}\text{if } i \neq i_s,\\ \text{if } i = i_s,\end{cases} \tag{77c}$$

$$C = \beta^2 A_3 + \tfrac{1}{2}\beta\Delta\xi A_5 + \begin{Bmatrix}(1-v)/2\\ \tfrac{1}{4}\end{Bmatrix}\beta A_2 \quad \begin{cases}\text{if } i \neq i_s,\\ \text{if } i = i_s,\end{cases} \tag{77d}$$

$$\text{RHS} = \begin{cases} -vA_1(Y_{i+1,j} + Y_{i-1,j}) + (1-v)A_1(2Y_{i-1,j} - Y_{i-2,j}) \\ \quad -\dfrac{v}{4}\beta A_2(Y_{i+1,j+1} - Y_{i+1,j-1} - Y_{i-1,j+1} + Y_{i-1,j-1}) \\ \quad +\dfrac{1-v}{2}\beta A_2(Y_{i-1,j+1} - Y_{i-1,j-1}) \\ \quad -\dfrac{v}{2}\Delta\xi A_4(Y_{i+1,j} - Y_{i-1,j}) + (1-v)\Delta\xi A_4\, Y_{i-1,j} \quad \text{if } i \neq i_s, \\ -A_1(Y_{i+1,j} - \alpha_j Y_{i-1,j} + \alpha_j Y_{i-2,j}) \\ \quad -\tfrac{1}{4}\beta A_2(Y_{i+1,j+1} - Y_{i+1,j-1} - 3Y_{i-1,j+1} + 3Y_{i-1,j-1} \\ \quad + Y_{i-2,j+1} - Y_{i-2,j-1}) \\ \quad -\tfrac{1}{2}\Delta\xi A_4(Y_{i+1,j} + \alpha_j Y_{i-1,j} - \alpha_j Y_{i-2,j}) \text{ if } i = i_s, \end{cases} \tag{77e}$$

$$\beta = \Delta\xi/\Delta\eta.$$

The boundary conditions are Dirichlet-type:

$$Y_{i,1}=\begin{cases} f(\xi_i) & \text{if } i_{\mathrm{LE}}\leqslant i\leqslant i_{\mathrm{TE}}, \\ 0 & \text{if } i<i_{\mathrm{LE}} \text{ or } i>i_{\mathrm{TE}}, \end{cases} \tag{77f}$$

$$Y_{i,j}=0 \quad \text{if } j=J_{\max} \text{ or } i=1 \text{ or } i=I_{\max}.$$

Applying Jones' transformation to equation (29), we get

$$B_1 R_\xi + B_2 R_\eta = B_3, \tag{78a}$$

where

$$B_1 = Y_\xi (Y_\eta + \psi_\eta)^2, \tag{78b}$$

$$B_2 = -(Y_\eta + \psi_\eta)(Y_\xi^2 + x_\xi^2), \tag{78c}$$

$$B_3 = (\gamma+1) M_\infty^2 \psi_\eta^2 \left(Y_{\xi\xi} - \frac{x_{\xi\xi}}{x_\xi} Y_\xi \right). \tag{78d}$$

The Crank–Nicolson scheme for equation (78a) produces the same form of difference equation, its coefficients and its RHS term as in equations (54a)–(54e), but the B's take a different form, i.e.

$$B_1 = \tfrac{1}{2}\{[Y_\xi (Y_\eta+\psi_\eta)^2]_{i,j} + [Y_\xi (Y_\eta+\psi_\eta)^2]_{i,j+1}\}, \tag{79a}$$

$$B_2 = -\tfrac{1}{2}\{[(Y_\eta+\psi_\eta)(Y_\xi^2+x_\xi^2)]_{i,j} + [(Y_\eta+\psi_\eta)(Y_\xi^2+x_\xi^2)]_{i,j+1}\}, \tag{79b}$$

$$B_3 = \frac{\gamma+1}{2} M_\infty^2 \left\{ \left[\psi_\eta^2 \left(Y_{\xi\xi} - \frac{x_{\xi\xi}}{x_\xi} Y_\xi \right) \right]_{i,j} + \left[\psi_\eta^2 \left(Y_{\xi\xi} - \frac{x_{\xi\xi}}{x_\xi} Y_\xi \right) \right]_{i,j+1} \right\}, \tag{79c}$$

and the ξ-derivatives Y_ξ and $Y_{\xi\xi}$ in equation (79c) should be approximated by a type-dependent difference scheme with SPOs

$$(Y_\xi)_{i,j} = \begin{cases} \dfrac{\nu}{2\Delta\xi}(Y_{i+1,j} - Y_{i-1,j}) + \dfrac{1-\nu}{\Delta\xi}(Y_{i,j} - Y_{i-1,j}) & \text{if } i \neq i_{\mathrm{s}}, \\ \dfrac{1}{2\Delta\xi}(Y_{i+1,j} - Y_{i,j} + \alpha_j Y_{i-1,j} - \alpha_j Y_{i-2,j}) & \text{if } i = i_{\mathrm{s}}, \end{cases} \tag{80a}$$

$$(Y_{\xi\xi})_{i,j} = \begin{cases} \dfrac{\nu}{\Delta\xi^2}(Y_{i+1,j} - 2Y_{i,j} + Y_{i-1,j}) + \dfrac{1-\nu}{\Delta\xi^2}(Y_{i,j} - 2Y_{i-1,j} + Y_{i-2,j}) & \text{if } i \neq i_{\mathrm{s}}, \\ \dfrac{1}{\Delta\xi^2}(Y_{i+1,j} - Y_{i,j} - \alpha_j Y_{i-1,j} + \alpha_j Y_{i-2,j}) & \text{if } i = i_{\mathrm{s}}. \end{cases} \tag{80b}$$

5. RESULTS AND DISCUSSION

The method developed here is used to calculate the transonic flows past symmetric aerofoils at zero angle of attack. Both subcritical and supercritical Mach numbers are considered. For unstretched co-ordinates (x, ψ) a 65×33 uniform mesh covers the domain $-2 \leqslant x \leqslant 3$, $0 \leqslant \psi \leqslant 2{\cdot}5$ and the aerofoil is located between 0 and 1 with 13 grid points on the surface. For stretched co-ordinates (ξ, η) a 65×33 uniform grid covers the computational domain $-1{\cdot}54 \leqslant \xi \leqslant 1{\cdot}54$, $0 \leqslant \eta \leqslant 1{\cdot}54$, corresponding to $-7{\cdot}04 \leqslant x \leqslant 7{\cdot}04$, $0 \leqslant \psi \leqslant 19{\cdot}47$. The aerofoil is located between $-0{\cdot}5$ and $0{\cdot}5$ and has 25 grid points on it (see Figure 5).

Most of the computations have been carried out on the y–R set of equations (28) and (29) for (x, ψ) co-ordinates and on the Y–R set of equations (72) and (78) for (ξ, η) co-ordinates. Other sets

of equations were only used for comparison with the y–R set. The relaxation parameters were taken as $\omega = 1{\cdot}7$–$1{\cdot}8$ for the subcritical case and $\omega = 0{\cdot}8$–$0{\cdot}9$ for the supercritical case.

Figure 6 shows the comparison of the calculated C_p-distribution of a 6% biconvex aerofoil at $M_\infty = 0{\cdot}909$ with experimental data.[27] The type-dependent difference scheme with SPO is used for the y-equation. We can see that the shock wave is very weak and accurately captured by the present scheme.

Figures 7–9 are comparisons of calculated NACA0012 C_p-distributions in (x, ψ) co-ordinates with experimental data at NAE[28] for $M_\infty = 0{\cdot}490$ and at ONERA[28] for $M_\infty = 0{\cdot}756$ and 0·803. In

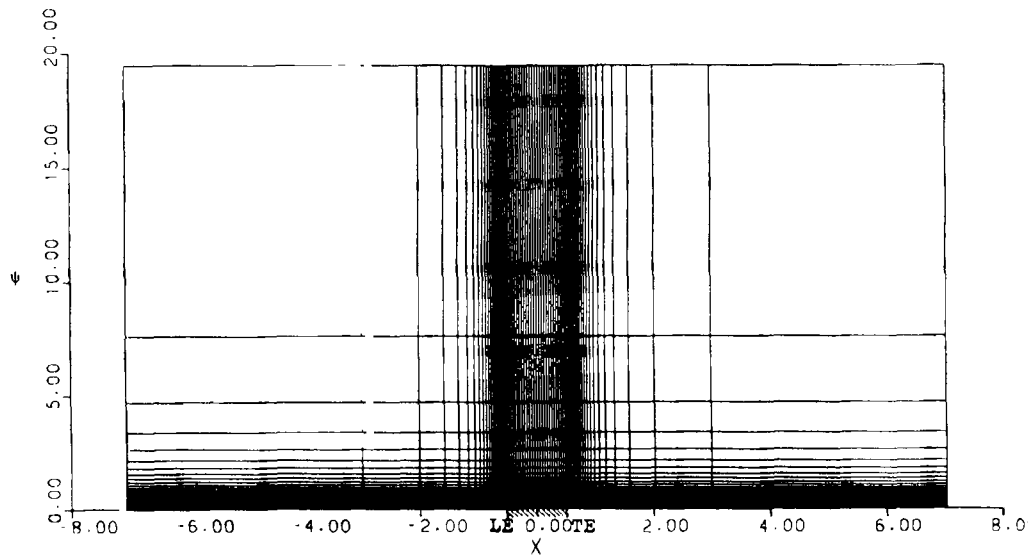

Figure 5. Grid system in (x, ψ) co-ordinates after Jones' stretching transformation; $x = ae^{-b\xi^2}\tan\xi$, $\psi = d\tan\eta$, $-1{\cdot}54 \leqslant \xi \leqslant 1{\cdot}54$, $0 \leqslant \eta \leqslant 1{\cdot}54$, $a = 0{\cdot}9$, $b = 0{\cdot}6$, $d = 0{\cdot}6$, $-7{\cdot}04 \leqslant x \leqslant 7{\cdot}04$, $0 \leqslant \psi \leqslant 19{\cdot}47$, $x_{LE} = -0{\cdot}5$, $x_{TE} = 0{\cdot}5$

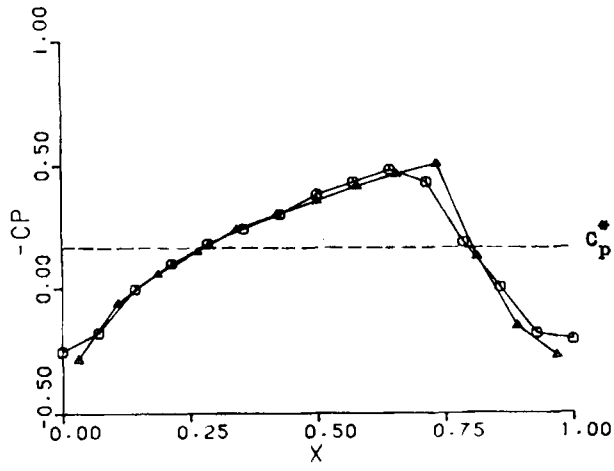

Figure 6. Comparison of pressure coefficient distribution with experimental data, 6% biconvex, $M_\infty = 0{\cdot}909$, y–R set: —Δ—, present; —○—, experimental data at NASA[27]

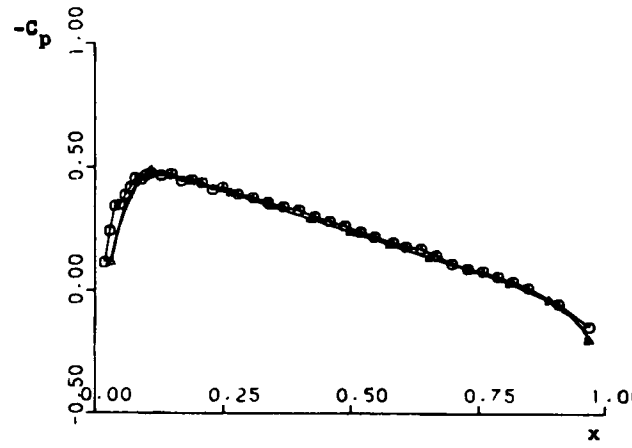

Figure 7. Comparison of pressure coefficient distribution with experimental data, NACA0012, $M_\infty = 0{\cdot}490$, y–R set: —Δ—, present; —○—, experimental data at NAE[28]

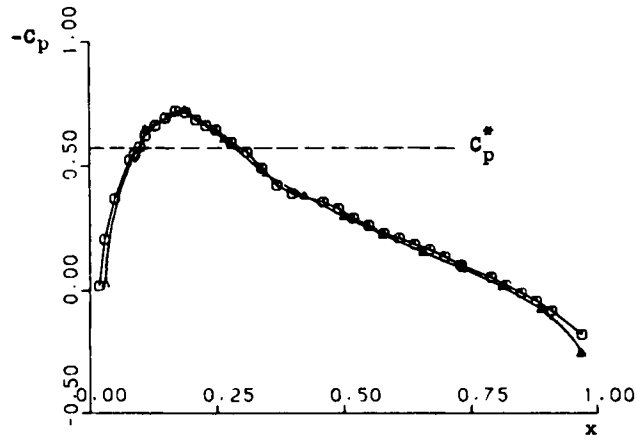

Figure 8. Comparison of pressure coefficient distribution with experimental data, NACA0012, $M_\infty = 0{\cdot}756$, y–R set: —Δ—, present; —○—, experimental data at ONERA[28]

order to show the improvement in accuracy using stretched co-ordinates, Figures 10 and 11 are comparisons of calculated C_p-distributions of NACA0012 with ONERA[28] for $M_\infty = 0{\cdot}803$ and NAE[28] for $M_\infty = 0{\cdot}817$. From these plots we can see that for both subcritical and supercritical cases the present approach gives good agreement with available experiments. For supercritical flow the shock wave location and strength are well predicted, but the shock is smeared out over two or three grid points sometimes and slight oscillation occurs after the shock wave.

Figure 12 shows the effect of the shock point operator in the y-equation on shock wave capturing for NACA0012 at $M_\infty = 0{\cdot}803$. Obviously, the type-dependent (TD) scheme with no SPO cannot correctly capture the shock wave and the C_p-distribution is incorrect, while the TD scheme with SPO is able to do so. Hence the SPO is a crucial tool to capture shock waves automatically.

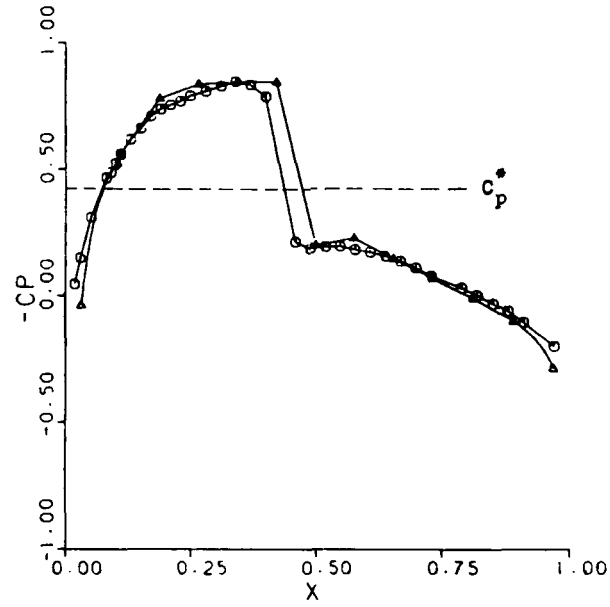

Figure 9. Comparison of pressure coefficient distribution with experimental data, NACA0012, $M_\infty = 0{\cdot}803$, y–R set: —Δ—, present, uniform grid; —○—, experimental data at ONERA[28]

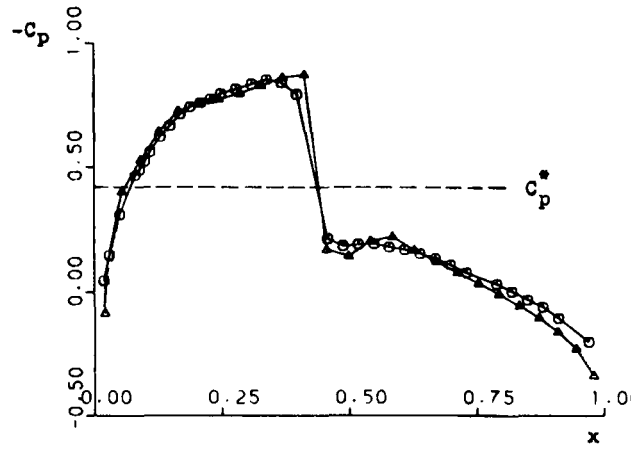

Figure 10. Comparison of pressure coefficient distribution with experimental data, NACA0012, $M_\infty = 0{\cdot}803$, Y–R set: —Δ—, present, clustered grid; —○—, experimental data at ONERA[28]

Figures 13–16 show the C_p-distributions for NACA0012 using various sets of equations: y–R with R_x given by (37), y–R with $L(y)=0$ and $L(R)=G$, y–M^2 and y–u–ρ. It was found that all the sets are capable of producing good results for subcritical flows. However, some difficulties are encountered in the computation for supercritical flows. Therefore the y–R set of equations (28) and (29) are recommended as an optimal set.

Figure 17 illustrates the convergence history of the R-equation. The horizontal axis gives the total number of iterations for y and the vertical axis is the logarithm of the error of R between two

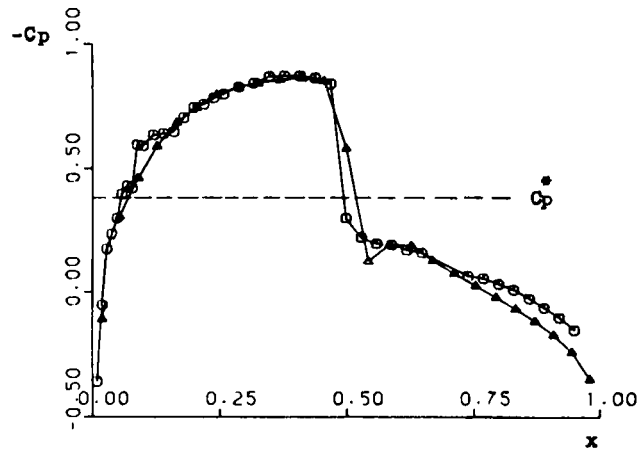

Figure 11. Comparison of pressure coefficient distribution with experimental data, NACA0012, $M_\infty = 0{\cdot}817$, Y–R set: —Δ—, present, clustered grid; —○—, experimental data at NAE[28]

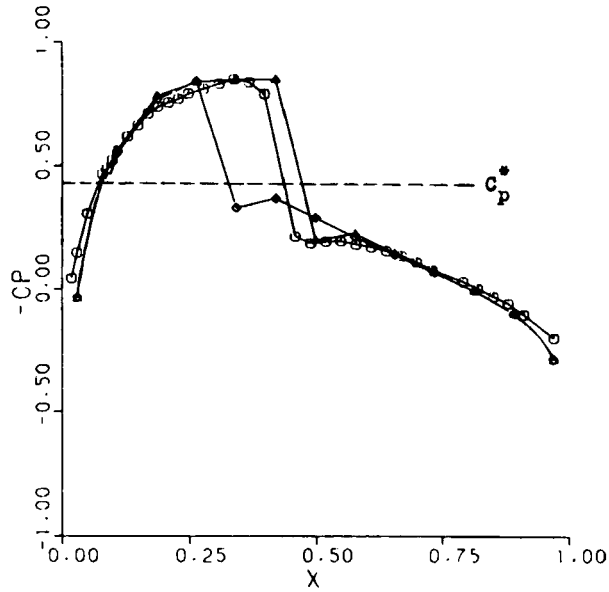

Figure 12. Effect of shock point operator (SPO) for y_{xx}, $y_{x\psi}$ on shock strength and location, NACA0012, $M_\infty = 0{\cdot}803$, y–R set: —Δ—, present; —○—, experimental data at ONERA;[28] —◇—, present without SPO

successive global iterations. For subcritical Mach number the convergence rate is fast and the maximum error decreases steeply, but for supercritical flow the convergence rate is much slower and the maximum error decreases slowly with violent oscillation.

Figure 18 indicates the effect of artificial density methods on the capturing of shock waves. Central differencing is used for both the y- and R-equations and a conventional artificial density $\tilde{R} = R - \mu R_x \Delta x$ is added. The result shows that the C_p-distribution is totally incorrect and the

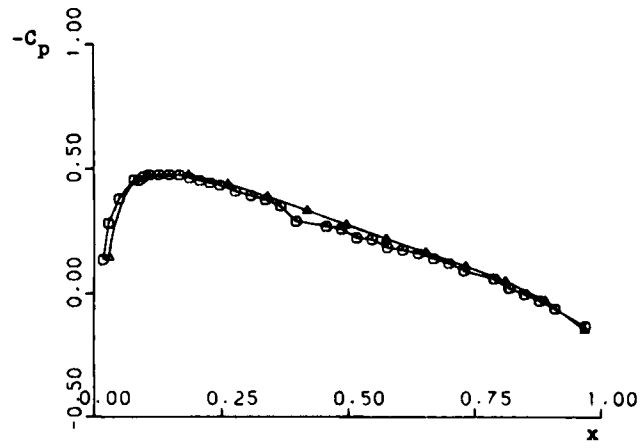

Figure 13. Comparison of pressure coefficient distribution with experimental data, NACA0012, $M_\infty = 0{\cdot}502$, y–R set, R_x given by (37): —Δ—, present; —○—, experimental data at ONERA[28]

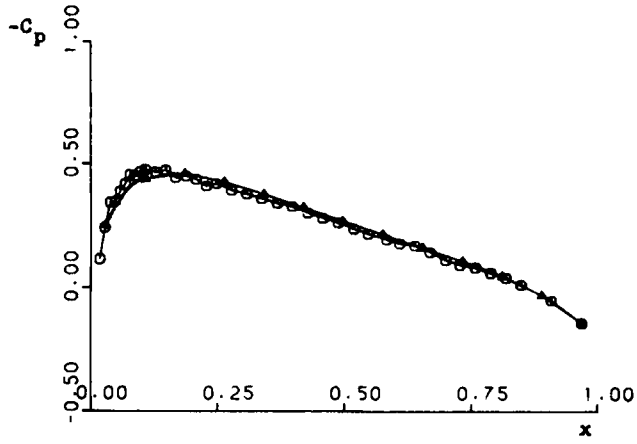

Figure 14. Comparison of pressure coefficient distribution with experimental data, NACA0012, $M_\infty = 0{\cdot}490$, y–R set, $L(y) = 0$, $L(R) = G$: —Δ—, present; —○—, experimental data at NAE[28]

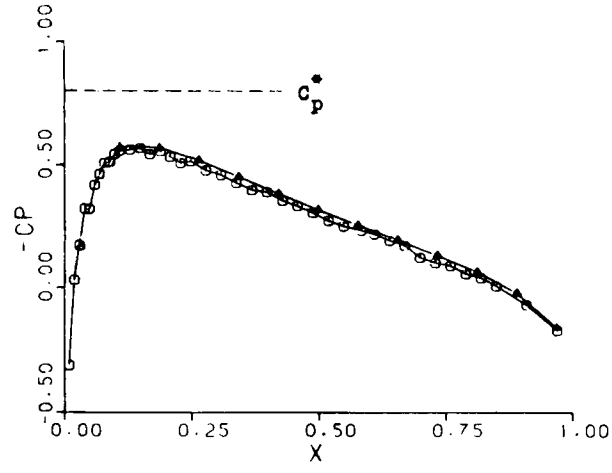

Figure 15. Comparison of pressure coefficient distribution with experimental data, NACA0012, $M_\infty = 0{\cdot}693$, y–M^2 set, $(M^2)_x$ given by (42): —Δ—, present; —○—, experimental data at NAE[28]

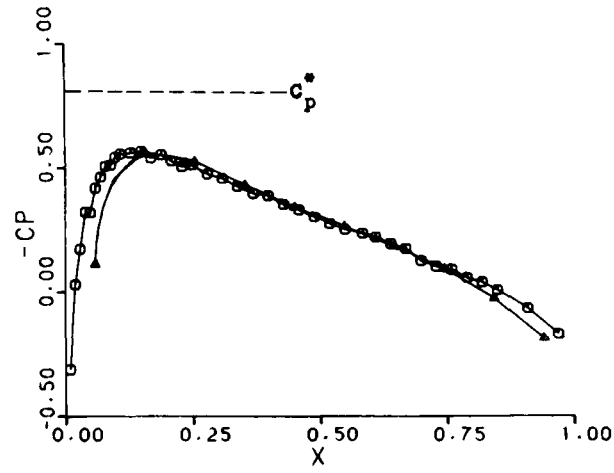

Figure 16. Comparison of pressure coefficient distribution with experimental data, NACA0012, $M_\infty = 0{\cdot}693$, y–u–ρ set: —△—, present; —○—, experimental data at NAE[28]

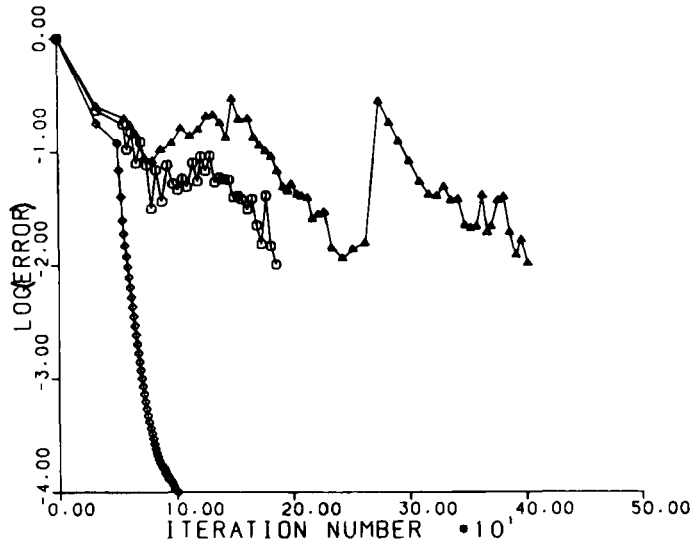

Figure 17. Convergence history for NACA0012: —◇—, $M_\infty = 0{\cdot}703$; —○—, $M_\infty = 0{\cdot}803$; —△—, $M_\infty = 0{\cdot}835$

shock wave is not captured. Hence it seems that the widely used artificial density technique in velocity potential computation is not easily extendable for our formulation.

Figure 19 is the comparison of the C_p-distribution for NACA0012 at $M_\infty = 0{\cdot}803$ for two difference schemes using the R-equation (29). One of them is the Crank–Nicolson scheme with TD and SPO for the y_{xx}-term in the R-equation. The other is TD with SPO for all y_{xx}-, y_x- and R_x-terms in the R-equation. It is clear that in the latter case the shock wave position and strength are highly oscillatory, while the former scheme gives accurate shock position and strength and less oscillation. Hence the first scheme is recommended.

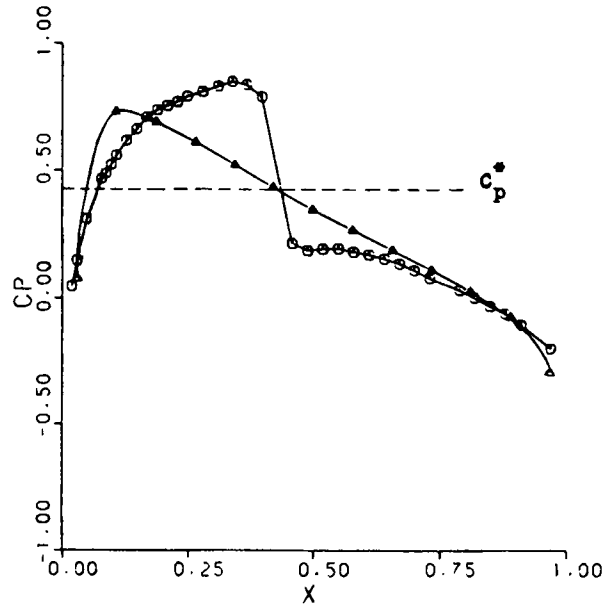

Figure 18. Inability of artificial density method to capture shock waves, NACA0012, $M_\infty = 0{\cdot}803$, y–R–$\tilde{R}$ set: —△—, artificial density method with central differencing; —○—, experimental data at ONERA[28]

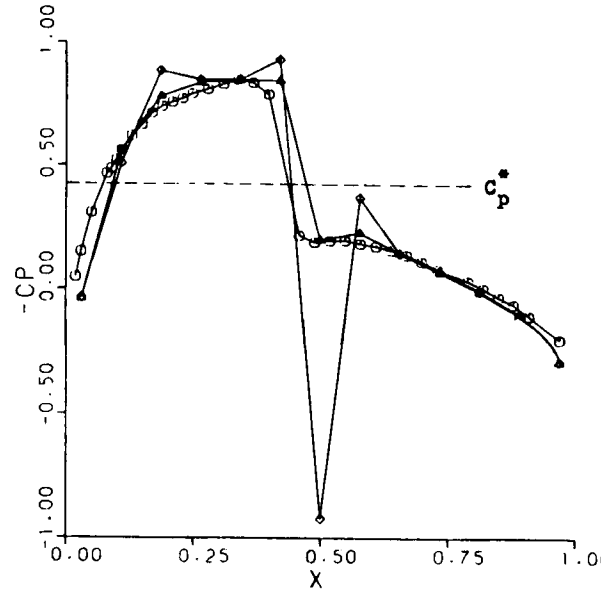

Figure 19. Effect of type-dependent (TD) differencing with shock point operator (SPO) for y_x, R_x, NACA0012, $M_\infty = 0{\cdot}803$, y–R set: —△—, present; —○—, experimental data at ONERA;[28] —◇—, present with y_x, R_x, TD + SPO

6. CONCLUDING REMARKS

1. The newly developed approach based on the full-potential-equivalent equations in von Mises co-ordinates, type-dependent scheme with shock point operator and successive line overrelation procedure is able to obtain accurate numerical solutions for both subcritical and supercritical transonic flows.
2. Embedded shock waves in supercritical flows can be captured automatically in the process of iteration and are smeared out over two or three grid points.
3. The full-potential-equivalent equations consist of a 'main' equation for the corresponding 'main' variable, which is the streamline ordinate y, and a 'secondary' equation for one of the following 'secondary' variables: density ρ, generalized density R, squared Mach number M^2, x-velocity component u, etc.
4. The type-dependent difference scheme with shock point operator (SPO) is effective to solve the 'main' equation for y and the SPO is crucial to capture shock waves, especially for moderate or strong ones.
5. Among various 'secondary' variables, their equations and a number of difference schemes, the generalized density R, its linear equation (29) and the Crank–Nicolson scheme are selected as an optimal combination to accompany the 'main' variable y and its equation.
6. The method developed here accurately captures shock waves in supercritical transonic flow without employing artificial dissipation schemes. This is advantageous, since the use of artificial density or viscosity requires a certain amount of tuning of the code, i.e. a number of parameters must be adjusted to achieve converged solutions. The present method, in which the only adjustable quantities are the relaxation parameters, is very robust and relatively easier to use.

ACKNOWLEDGEMENT

The authors thank the Natural Science and Engineering Research Council of Canada for financially supporting this project.

REFERENCES

1. E. M. Murman and J. D. Cole, 'Calculation of plane steady transonic flows', *AIAA J.*, **9**, 114–121 (1971).
2. E. M. Murman and J. A. Krupp, 'Solution of the transonic potential equation using a mixed finite difference system', *Lecture Notes in Physics*, Vol. 8, Springer, Berlin, 1971, pp. 199–206.
3. E. M. Murman, 'Analysis of embedded shock waves calculated by relaxation methods', *AIAA J.*, **12**, 626–633 (1974).
4. M. Hafez and H. K. Cheng, 'Shock fitting applied to relaxation solutions of transonic small disturbance equations', *AIAA J.*, **5**, 786–793 (1977).
5. D. J. Jones and R. G. Dickinson, 'A description of the NAE two-dimensional transonic small disturbance computer method', *NAE Laboratory Technical Report LTR-HA-39*, January 1980.
6. A. Jameson, 'Iterative solution of transonic flows over airfoils and wings, including flow at Mach 1', *Commun. Pure Appl. Math.*, **27**, 283–309 (1974).
7. A. Jameson, 'Numerical solution of transonic flows with shock waves', *Symp. Transsonicum II*, Springer, Berlin, 1976, pp. 384–414.
8. M. Hafez, J. South and E. M. Murman, 'Artificial compressibility methods for numerical solution of transonic full potential equations', *AIAA J.*, **17**, 838–844 (1979).
9. W. G. Habashi and M. Hafez, 'Finite element solutions of transonic flow problems', *AIAA J.*, **20**, 1368–1378 (1982).
10. M. Hafez and D. Lovell, 'Improved relaxation schemes for transonic potential calculations', *Int. j. numer. methods fluids*, **8**, 1–6 (1988).
11. R. Magnus and H. Yoshihara, 'Inviscid transonic flow over airfoils', *AIAA J.*, **8**, 2157–2162 (1970).
12. R. M. Beam and R. F. Warming, 'An implicit finite difference algorithm for hyperbolic system in conservation law form', *J. Comput. Phys.*, **22**, 87–110 (1976).
13. J. C. Steger, 'Implicit finite difference simulation of flow around arbitrary two-dimensional geometries', *AIAA J.*, **16**, 676–686 (1978).

14. T. H. Pulliam and D. S. Chaussee, 'A diagonal form of an implicit approximate factorization algorithm', *J. Comput. Phys.*, **39**, 343–383 (1981).
15. A. Jameson, W. Schmidt and E. Turkel, 'Numerical solutions of the Euler equations by finite-volume methods using Runge–Kutta time-stepping schemes', *AIAA Paper 81-1259*, 1981.
16. R. H. Ni, 'A multi-grid scheme for solving the Euler equations', *AIAA J.*, **20**, 1565–1571 (1982).
17. W. G. Habashi and M. Hafez, 'Finite element stream function solutions for transonic turbomachinery flows', *AIAA Paper 82-1268*, 1982.
18. M. Hafez and D. Lovell, 'Numerical solution of transonic stream function equation', *AIAA J.*, **21**, 327–335 (1983).
19. W. G. Habashi, P. L. Kotiuga and L. A. McLean, 'Finite element simulation of transonic flows by modified potential and stream function methods', *Eng. Anal.*, **2**, 150–154 (1985).
20. H. L. Atkins and H. A. Hassan, 'A new stream function formulation for the steady Euler equations', *AIAA J.*, **23**, 701–706 (1985).
21. R. M. Barron, 'Computation of incompressible potential flow using von Mises coordinates', *J. Math. Comput. Simul.*, **31**, 177–188 (1989).
22. M. H. Martin, 'The flow of a viscous fluid I', *Arch. Rat. Mech. Anal.*, **41**, 266–286 (1971).
23. R. M. Barron and R. K. Naeem, 'Numerical solution of transonic flows on a streamfunction coordinate system', *Int. j. numer. methods fluids*, **9**, 1183–1193 (1989).
24. R. K. Naeem and R. M. Barron, 'Transonic computation on a natural grid', *AIAA J.*, **28**, 1836–1838 (1990).
25. G. S. Dulikravich, 'A stream-function-coordinate (SFC) concept in aerodynamic shape design', *AGARD VKI Lecture Series* (1990).
26. M. S. Greywall, 'Streamwise computation of 2-D incompressible potential flows', *J. Comput. Phys.*, **59**, 224–231 (1985).
27. E. D. Knetchtel, 'Experimental investigation at transonic speeds of pressure distributions over wedge and circular-arc-airfoil sections and evaluation of perforated wall interference', *NASA TN D-15*, 1959.
28. J. J. Thibert, M. Grandjacques and L. H. Ohman, 'Experimental data base for computer program assessment', *AGARD AR-138*, 1979, pp. A1-1–A1-36.